J Ther Eng, Vol. 12, No. 2, pp. 796−813, March, 2026

Journal of Thermal Engineering
Web page info: https://jten.yildiz.edu.tr
DOI: 10.14744/thermal.0001119

Research Article

Numerical analysis of two-phase flow in u-bend pipes: effects of curvature, and pipe orientation on pressure drop and liquid hold-up

Md. Zahid HASAN[1], Dipayan MONDAL[1,*], Mihir Ranjan HALDER[1]

[1]*Department of Mechanical Engineering, Khulna University of Engineering & Technology, Khulna, 9203, Bangladesh*

ARTICLE INFO

Article history
Received: 11 January 2025
Revised: 07 April 2025
Accepted: 12 April 2025

Keywords:
Two-phase Flow; U-bend Pipe; Pressure Drop; Phase Distribution; Liquid hold-up; VOF Model

ABSTRACT

This work investigates the effects of bend curvature, pipe orientation, and bend angle on two-phase flow dynamics in U-bend tubes using a numerical approach. Two-phase flow in U-bend tubes introduces secondary flows, significantly impacting pressure drops and phase distributions. This study employs numerical simulations using ANSYS Fluent 2020 R1® to analyze the effects of bend curvature and pipe orientation (horizontal and vertical) on flow behavior, with water and air as the working fluids at an inlet velocity of 3 m/s. The volume of fluid model was employed to capture phase interactions and this is the novelty of this present work as in the previous works, the use of this model was absent. Results reveal a wavy stratified flow with secondary vortices caused by centrifugal forces in the bend. Pressure losses of 1186 Pa and 1415 Pa were observed for 50% and 70% water volume fractions in the vertical orientation, while horizontal orientation exhibited negligible losses for 50% and 80 Pa for 70%. Consequently, the pressure losses were found higher in vertical orientations, with 50% and 70% water volume fractions, respectively. The pressure drop is observed more with a higher bend angle along the bend. This Increased liquid hold-up and water accumulation at the bend were observed with higher water fractions, contributing to greater pressure drops. These findings are critical for applications in oil and gas, chemical processing, and refrigeration, highlighting the need for further studies on flow patterns and alternative geometries. The flow pattern as well as can significantly affect the overall flow behavior.

Cite this article as: Hasan MZ, Modal D, Halder MR. Numerical analysis of two-phase flow in u-bend pipes: effects of curvature, and pipe orientation on pressure drop and liquid hold-up. J Ther Eng 2026;12(2):796−813.

INTRODUCTION

This study aims to investigate the effects of curvature, orientation, and phase interactions on pressure drop and liquid hold-up in U-bend pipes. Multiple phases of flowing fluid are observed in different industries such as refrigeration, oil and gas, etc. In these areas, phases can change from one state to another, or two different types of phases such as gas-liquid, liquid-solid, or solid-gas can be observed. For the flowing of the phases, straight pipes as well as different types of bend are used such as 90-degree

***Corresponding author.**
*E-mail address: dipkuet@me.kuet.ac.bd

This paper was recommended for publication in revised form by Editorin-Chief Ahmet Selim Dalkılıç

bend angle, and U-bend pipe. In most cases, U-bend pipe is used extensively. The bending curvature, orientations of the pipe, phase distributions through the pipe, etc. are significant factors in analyzing the fluid flow behavior. Hence, the present work is performed based on this vital factor. Before, the extensive literature review was conducted to work on specific research gaps which have been discussed in the preceding parts. Hayashi et al. [1] experimentally investigated the pressure drop of air-water two-phase flow in a horizontally oriented U-bend pipe. Dassler and Janoske [2] investigated the effect of the radius of curvature on the pressure drop both experimentally and numerically for rectangular-shaped U-bends placed horizontally. However, Pham et al. [3] performed a numerical investigation at four different orientations of the pipe. Again, placing a horizontal-vertical plane, Hayashi et al. [4] checked the effect of bend on a void fraction of two-phase flow. Similarly, Yadav and Mehta [5] investigated the influence of the radius of curvature on a horizontally oriented mini-channel U-bend pipe. In contrast, Usui et al. [6] analyzed two-phase flow behavior in an inverted U-bend pipe. Da Silva Lima [7] made an analysis of two-phase flow in three pipe orientations such as horizontal, vertical up-flow, and vertical down-flow using R134a refrigerant. Deng et al. [8] used nitrogen-water two phases to perform flow analyses at the horizontal position. Aliyu et al. [9] utilized serpentine construction positioning horizontally with a larger diameter of U-bend pipe to analyze gas-liquid two-phase flow behavior. Monachen et al. [10] numerically investigated air-water flow behavior in a straight channel unlikely the U-bend pipe.

De Moerloose et al. [11] performed a simulation of the effect of the liquid viscosity, wall wetting, and mass flow through a horizontal U-bend pipe using an air-water mixture. However, Ma et al. [12] investigated the perturbation length of vertical U-bend pipe using the air-water mixture. Unlike the literature, Mondal et al. [13] and Ghosh et al. [14] used single-phase flow and oil-water mixture in a U-bend pipe respectively. Another numerical work performed by Bandyopadhay and Das [15] using a U-bend pipe at a horizontal position used air-water in two phases. A comparative investigation was conducted by Andrzejczyk and Muszynski [16] between U-bend and straight pipes at vertical positions. Ogunsesan et al. [17] developed a CFD modeling for double elbow geometry for air-water two-phase flow. Pressure drop analysis of air-water two-phase flow through a 90-degree vertical pipe was performed by Saber and Maree et al. [18]. Using an air-water mixture, Zahedi and Rad [19] investigated both numerically and experimentally to observe the flow behavior in a 90-degree bend pipe. On the other hand, Lopez et al. [20] used a horizontal U-bend pipe to observe the liquid film behavior of the air-water annular flow.

Lu et al. [21] experimentally investigated an air-water mixture through a straight channel. Abdulkadir et al. [22] investigated how liquid film thickness changed at the U-bend at different angles by using an air-water mixture. Nouri et al. [23] numerically investigated oil-water two-phase flow through the straight channel. Mahmood et al. [24] also used a straight channel to investigate the effect of two-phase flow development incorporating an expansion device. Karademir et al. [25] comprehensively reviewed two-phase flow behavior using an inclined tube. Yaqop [26] experimentally and numerically studied the pressure drop of air-water two-phase flow through straight flattened tubes. Hamad et al. [27] investigated experimentally and compared the data with numerical work using a kerosene-water two-phase flow in a 90-degree bend tube instead of an air-water mixture. Mondal et al. [28] used Silicon oil and air-water to understand the flow behavior in an intermediate vertical tube. Air-water and air-water-oil three-phase flows were observed by Spedding et al. [28] in a 90-degree bend pipe. Effects of heat transfer using two different refrigerants along with nano-particles in a U-bend pipe were investigated by Islam et al. [29].

Jiang et al. [30] numerically investigated two oil-water phases in a U-bend pipe using core annular flow. Ooms et al. [31] performed a numerical investigation of core annular flow in a 90-degree bend pipe. Ma et al. [32] examined ice slurry flow through a horizontally placed elbow pipe. Onal et al. [33] investigated heat transfer and pressure drop characteristics of two-phase flows using helical coils. Govier and Omer [34] investigated air-water two-phase flow to observe pressure drop, and liquid holdup in a horizontal pipe. Similarly, friction characteristics and two-phase flow patterns were investigated in a smooth tube by Wang et al. [35]. Again, Wang et al. [36] investigated the return bend effect of a horizontally placed tube using the air-water mixture. The oil-water two-phase flow was investigated in a microchannel by Salim et al. [37]. Al-Hadhrami et al. [38] experimentally investigated air-water-oil three-phase flow in a straight pipe to study the flow regimes and pressure gradient. Patpatiya et al. [39] investigated numerically two-phase flow in a T-junction tube placed horizontally. Lightstone et al. [40] experimentally and numerically investigated air-water two-phase flow in a horizontal smooth tube with dividing sections. Nizovtseva et al. [41] numerically observed a two-phase flow in a closed bioreactor loop. Verma and Ghosh [42] compared gas-liquid and liquid flows through mini-channel tubes. Meanwhile, Mondal et al. [43,44], conducted the parallel, counter, and cross-flow water-to-air u-bend heat exchanger and also a cooling system adopted by the vapor absorption system, while Mondal and Islam [45] reported another study for intermittent system adopted by ammonia absorption refrigeration system. To fit the refrigerants in HVAC&R systems, Mondal et al. [46-49] and Islam et al. [29], measured the transport properties as well as the heat transfer characteristics of several refrigerants that will take in the future revolution of industries. Moreover, Das et al. [50] and Arefin et al. [51] evaluated the thermodynamic analysis of the dual and single cascading vapor compression cycle, respectively, for the low-temperature application. Moreover, Bari et al. [52] presented the

analysis of heat transmission in a refrigerant compartment, while Shahariar et al. [53] represented the performance of LiCl desiccant dehumidifier. Akinshilo and Sobamowo [54] analyzed pipe flow, heat transfer characteristics, and entropy generation in fourth-grade fluid with temperature dependent viscosities and heat generation using the regular perturbation method. The results showed ways to advance the analysis and process behavior of the fourth-grade fluid flow and steady-state heat transfer processes such as those found in petroleum, polymer, food manufacturing, and paint industries. Akinshilo and Olaye [55] investigated the flow and heat transfer of a non-Newtonian Erying Powell fluid flow in a pipe. Obtained solutions may be used to advance studies in thin film flow, polymer processing and paper production. Akinshilo and Sobamowo [56] studied the flow, thermal and concentration analyses of blood as a third grade with gold as nanoparticles through a porous channel using regular perturbation method. The outcomes can be utilized to advance the study of blood transport in porous channels with nanoparticles which acts as an effective drug delivery mechanism in the treatment of blood-related diseases. Sheikh et al. [57] investigated the combined influence of the nanoparticles and uniform magnetic field applied on the slip blood flow. The results revealed the augmentation of the pressure gradient and the magnetic parameter decreased the velocity value whilst the viscous dissipation augmentation increased the temperature.

According to the pipe orientations, the pressure, phase distribution, and liquid film thickness vary which has been observed through the above studies. From the above literature study, it can be said that the majority of the studies have been focused on the horizontal orientations of the U-bend tube. Additionally, some of the works have been done using other geometries while the U-bend tube is one of the most used channels in different industries mentioned before. Pressure drops, liquid hold-up, volume fractions, etc. have been solely investigated using horizontal orientation. Investigations on other orientations are needed to observed. The major research objective is to observe how pipe orientations can effectively influence different parameters during two-phase flow. Hence, two pipe orientations are numerically simulated to describe which orientation of the pipe can cause more pressure drop and influence other parameters. Though experimental analyses have been performed, numerical solutions can be viable and may be the best ones. So, in this present work, the numerical solution is hoped to replace the experimental ones. The novelty of this present work is to use the volume of fluid method for capturing the water-air phase interactions during the simulation. So, the present study is focused on the different pipe orientations of U-bend tubes notably vertical-horizontal and vertical to investigate the pressure variation, phase distribution, liquid thickness, and effect of bend angle on pressure variation at the bend in a U-bend pipe.

METHODOLOGY

The present work is performed using the finite volume method (FVM). This section explains the numerical techniques and models used to analyze two-phase flow in U-bend pipes, with an emphasis on how phase interactions, curvature, and orientation affect liquid hold-up and pressure drop.

Numerical Model

The Reynolds Averaged Navier-Stokes (RANS) equations are utilized in turbulence modeling. For the steady-state flow conditions, the Reynolds Averaged Navier-Stokes continuity, momentum equations are as follows [58],

Continuity equation:

$$\frac{\partial}{\partial x_i}(\rho u_i) = 0 \tag{1}$$

Momentum equation:

$$\frac{\partial}{\partial x_j}(\rho u_i u_j) = -\frac{\partial p}{\partial x_i} + \frac{\partial}{\partial x_j}\left[\mu\left(\frac{\partial u_i}{\partial x_j} + \frac{\partial u_j}{\partial x_i} - \frac{2}{3}\delta_{ij}\frac{\partial u_l}{\partial x_l}\right)\right] + \frac{\partial}{\partial x_j}(-\rho\overline{u_i u_j}) \tag{2}$$

Where, ρ = density, and u_i, u_j = velocity.

Governing equations

The continuity, momentum, and volume fraction equations which are resolved throughout the numerical simulation are the governing equations for the volume of fluid model (VOF). The continuity equation has been used for the conservation of mass. The momentum equation is for the velocity of the water and air phases. Next, for incorporating and capture the two phase flow phenomenon, the volume fraction equations have been incorporated.

The continuity equation is as follows [23],

$$\nabla(\rho v)=0 \tag{3}$$

Where, ρ is the density of the mixture

The volume fraction equation [58],

$$\nabla.\left(\alpha_q \rho_q . \overrightarrow{v_q}\right) = 0 \tag{4}$$

Where, α_q = volume fraction.

Based on the following equation, the volume fraction equation is solved for the secondary phase but not for the main phase.

$$\sum_{q=1}^{n} \alpha_q = 1 \tag{5}$$

Momentum equation [58],

$$\nabla.(\rho v \vec{v}) = -\nabla p + \nabla.[\mu(\nabla\vec{v} + \nabla(\vec{v})^T)] + \rho\vec{g} + \vec{F} \tag{6}$$

Where, $\vec{v}$ = velocity, $\vec{F}$ = force.

In addition, wall adhesion and the continuum surface force model are solved for the introduction of surface

tension. Again, the surface tension is viewed as a continuous, three-dimensional effect rather than a boundary value in Brackbill et al.'s [59] continuum surface force model. Surface tension can be computed by adding a source term to the momentum equation. The normal forces are then taken into consideration, and the surface tension is treated as a constant along the surface to determine the source term's origin.

The pressure drops depending on the surface tension and the surface curvature radii taking in the orthogonal direction can be calculated as

$$p_2 - p_1 = \sigma(\frac{1}{R_1} + \frac{1}{R_2}) \tag{7}$$

Where p_2 and p_1 are the two pressures in the two fluids on either side of the interface.

Local gradients normal to the interface are used to calculate the surface curvature.

$$n = \nabla \alpha_q \tag{8}$$

Where n is the surface normal correlated to the gradient of q^{th} volume fraction. Now, the curvature is correlated by the divergence of the unit normal $\hat{n}$ [59].

$$\kappa = \nabla . \hat{n} \tag{9}$$

where, $\hat{n} = \frac{n}{|n|}$

The momentum equation for the surface tension inclusion is expanded to include the volume force as the source term and it is as follows,

$$F_{vol} = \sum_{pairsi\ j,i<j} \sigma_{ij} \frac{\alpha_i \rho_i \kappa_j \nabla \alpha_j + \alpha_j \rho_j \kappa_i \nabla \alpha_i}{\frac{1}{2}(\rho_i + \rho_j)} \tag{10}$$

For two-phase flows, the above volume force can be written as,

$$F_{vol} = \sigma_i j \frac{\rho \kappa_i \nabla \alpha_i}{\frac{1}{2}(\rho_i + \rho_j)} \tag{11}$$

Where, ρ is the volume averaged density.

The effect of wall adhesion is incorporated into the continuum surface force model by defining the contact angle between the fluid and the wall to the surface normal to the near wall and the surface normal can be denoted as,

$$\hat{n} = \widehat{n_w} cos\theta_w + \widehat{t_w} sin\theta_w \tag{12}$$

where, $\widehat{n_w}$ and $\widehat{t_w}$ are the unit vectors normal and tangential to the wall.

The RNG k-ε turbulence model is used. The transport equation of two fluid steady states is as follows,

$$\frac{\partial}{\partial x_i}(\rho k u_i) = \frac{\partial}{\partial x_j}\left(\alpha_k \mu_{eff} \frac{\partial k}{\partial x_j}\right) + G_k + G_b - \rho\varepsilon - Y_M + S_K \tag{13}$$

$$\frac{\partial}{\partial x_i}(\rho \epsilon u_i) = \frac{\partial}{\partial x_j}\left(\alpha_\varepsilon \mu_{eff} \frac{\partial \varepsilon}{\partial x_j}\right) + C_{1\varepsilon} \frac{\varepsilon}{k}(G_k + C_{3\varepsilon} G_b) - C_{2\varepsilon} \rho \frac{\varepsilon^2}{k} - R_\varepsilon + S_\varepsilon \tag{14}$$

Taking, $C_{1\varepsilon}$ = 1.42, $C_{2\varepsilon}$ = 1.68. Where, G_k is the turbulence kinetic energy due to the mean velocity gradients, G_b is the generation of turbulence kinetic energy due to buoyancy, Y_M is the contribution of the fluctuating dilatation in compressible turbulence to the overall dissipation rate, α_k is the inverse Prandtl number for k, α_ε is the inverse Prandtl number for ε, and S_K, S_ε are considered as the user-defined source term.

For near-wall treatment, standard wall function is used along with the k-ε turbulence model as this wall treatment is widely used for industrial applications. The equations are as follows,

Momentum equation,

$$U^* = \frac{1}{\kappa} ln(E y^*) \tag{15}$$

Where, U^*= dimensionless velocity, y^*= dimensionless distance from the wall.

$$U^* = \frac{U_P C_\mu^{1/4} K_P^{1/2}}{\tau_w / \rho} \tag{16}$$

$$y^* \equiv \frac{\rho C_\mu^{1/4} K_P^{1/2} y_P}{\mu} \tag{17}$$

Physical Domain

Two geometrical orientations namely vertical-horizontal and vertical have been used in this numerical investigation. These two orientations are widely used for industrial purposes. Hence, the pipe orientations are chosen. The length of the straight pipe is 560 mm, the bend radius is 125 mm, the pipe diameter is 28 mm, and these measurements were taken by Pham et al. [3]. Figure 1(a) shows the labeling of the U-bend tube. The dimension of the pipe starts at 0 mm from the inlet. Dividing the pipe into several parts, the axial position is used for the pressure variation axially of the pipe. The total axial length of the U-bend pipe is approximately 1512.7 mm and the end is at the outlet of the pipe. The curvature length is 392.7 mm which is calculated by π times the radius of the curvature of the bend portion. In this study, the position of the U-bend tube pipe is considered in two types of orientations: horizontal-vertical orientation and vertical orientation shown in Figure 1(b) and Figure 1(c), respectively.

Boundary Conditions and Solver Setting

The inlet face is divided into 30% air, 70% water, and 50% for both water and air, in order to enforce the inlet boundary criteria. The gauge pressure, which has a value of zero Pascal, is the outlet pressure. The atmospheric pressure, which has a value of 101325 pascals, is the operating

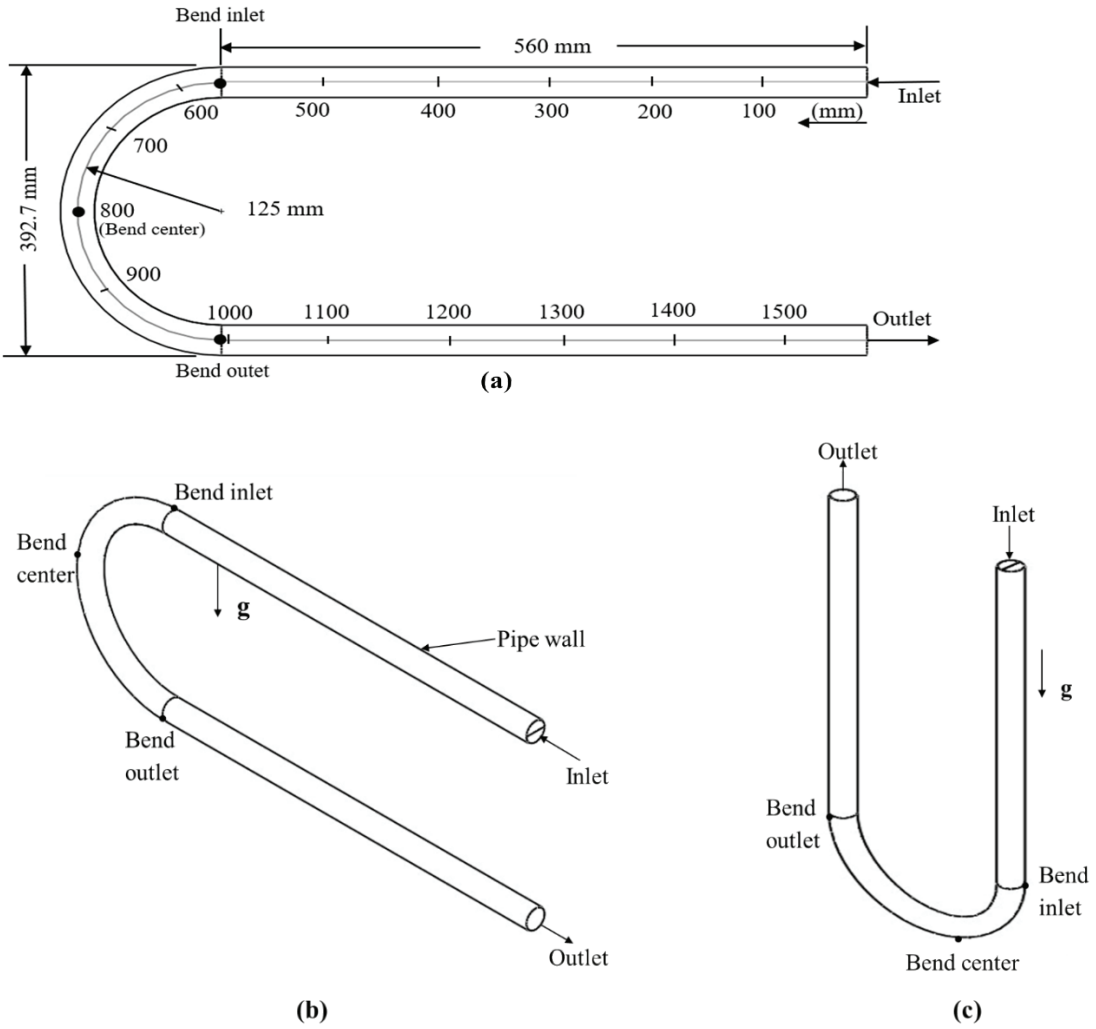

Figure 1. Illustration of the U-bend pipe: (a) geometry labeling, (b) horizontal-vertical orientation, and (c) vertical orientation.

pressure. The operational density of the lightest fluid air is selected as 1.225 (kg/m^3). Determining the volume fraction 1 at the split part of the inlet face yields an inlet velocity of 3 m/s for both water and air. To avoid slip between the air-water interface, the same velocity has been chosen for both fluids. The volume fractions are chosen to avoid complexity during the simulation. A brief description of the other boundary conditions is shown in Table 1 below.

The solver setup utilized for the numerical investigation is displayed in Table 2 along with a brief description. Applying a pressure-based solution, water and air are considered incompressible fluids. The pressure-based solution considers the fluids incompressible. Hence it is incorporated. Next, the gravitational acceleration in the negative z direction is used in the steady state condition (-9.81 m/s^2). Furthermore, the implicit volume fraction parameters with

Table 1. Boundary conditions for the U-bend pipe

Items	Description	Items	Description
Primary phase	Water	Wall condition	No slip stationary wall
Secondary phase	Air	Wall adhesion	90-degree contact angle
Water velocity, v_l	3 m/s	Surface tension, σ	0.072 N/m
Air velocity, v_a	3 m/s	Outlet	Pressure outlet
Volume of fractions, α	0.5, 0.7		

Table 2. Numerical setting for the investigation

Items	Description	
Solver type	Pressure Based Solver	
Condition	Steady State	
Gravity	On	
Multiphase model	Volume of Fluid	
Implicit body force	On	
Interface modeling	Sharp	
Turbulence model	k-ε (K-Epsilon)	
Near wall treatment	Standard wall functions	
Solver method	Pressure-velocity coupling: Coupled	
Initialization	Standard initialization	
Transient formulation	Pseudo Transient	
Residual	Continuity	10^{-2}
	Momentum	10^{-4}
	k	10^{-3}
	epsilon	10^{-2}
	Vf-air	10^{-3}
Spatial Discretization	Gradient	Least square cell-based, Green Gauss node-based
	Pressure	PRESTO
	Momentum	First order upwind
	Volume fraction	Compressive
	Turbulent kinetic energy and dissipation rate	First order upwind

the body force are implied because of the steady state. A sharp interface is taken for the stratified flow through the tube in order to capture the contact between the air and water phases. So, the volume of the fluid model has been chosen. Additionally, the coupled pressure-velocity technique with first-order upwind discretization is selected for improved convergence as the most economical solution. The reduced residuals make the solution more viable and less erroneous. However, in this present study, in spite of the present simulation's reduced residuals, the data obtained after all residuals remain constant for an extended period of time. Furthermore, the findings are derived based on the residuals being kept constant with reduced fluctuations after 1000 iterations. To avoid convergence errors, the constant values in the RNG k-e models have been modified as per the guidance of the theory. Furthermore, the findings revealed tendencies that were consistent with previous experimental studies. However, the two-phase flow simulations' complexity may have led to a convergence issue with smaller residuals.

Mesh Independency and Validation

After designing in the design software via ANSYS Fluent 2020 R1, the U-bend pipe is imported into the Meshing software. The U-bend pipe has been discretized into three-dimensional tetrahedron meshing. The unstructured tetrahedron meshing with patch-conforming mesh method has been applied. This is due to the fact that the tetrahedron meshing with the patch-conforming method requires less time than the more structured hexahedron mesh. However, Figure 2 shows the grid discretization of the U-bend pipe, while the mesh element size along with other details have been presented in Table 3.

The grid independence test is performed to ascertain whether or not the outcome is grid-dependent for the validation, while Figure 3 illustrates the mesh independence test. For element sizes of 1.25 mm and 1.50 mm with different numbers of mesh elements, the maximum water velocity

Table 3. Meshing elements

Items	Description
Type of Mesh	Tetrahedral
Mesh Method	Patch Conforming Method
Element Size	1.5 mm
No of Elements	2154936
No of Nodes	778390
Inflation Layer	8
First Layer Thickness	0.04mm
Wall Y^+	Min: 2.20, Max: 2.97

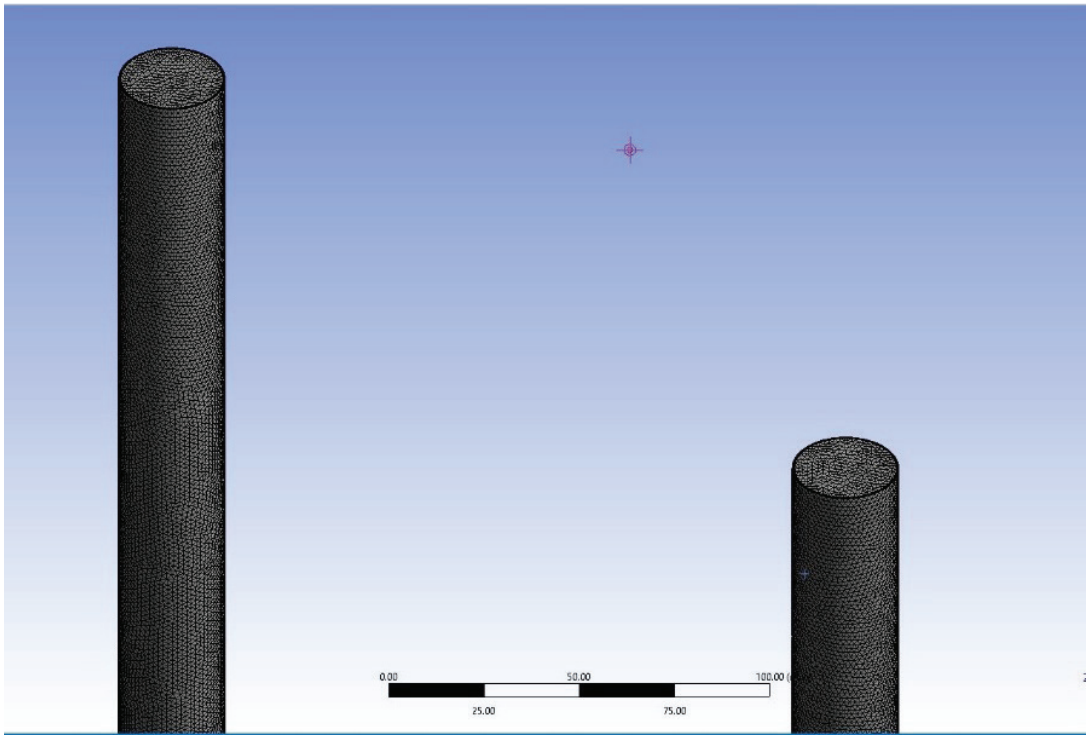

Figure 2. Grid discretization of the U-bend pipe.

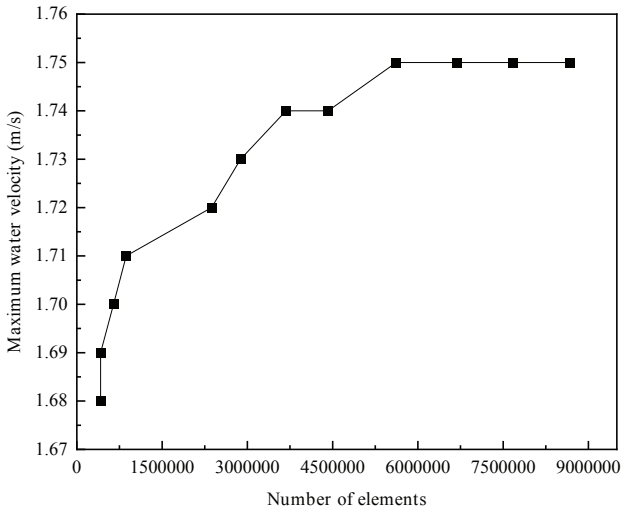

Figure 3. Grid independence test.

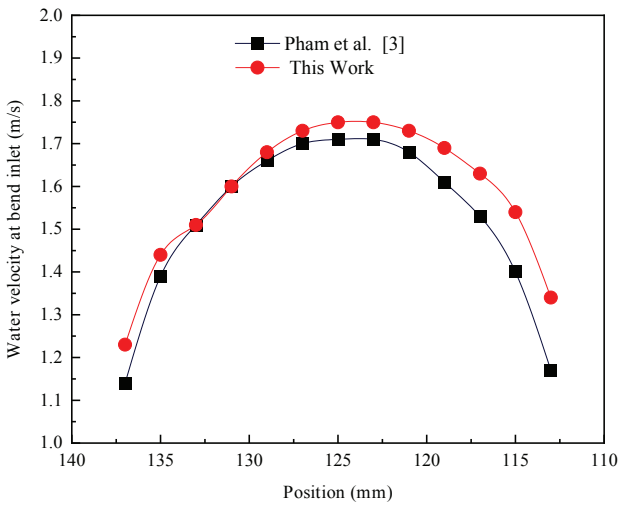

Figure 4. Numerical model validation.

of 1.75 m/s is investigated. For 1.25 mm and 1.50 mm, the outcomes are comparable. However, for a numerical solution that is computationally economical, the element size of 1.50mm is selected; otherwise, the computational cost would be high for the same result. Again, Figure 4 shows the model validation numerically. Validation is performed to increase the acceptability of the numerical analysis as well as the results. The SST k-ω turbulence model is used for the validation. The mixture model for the two-fluid models given by Pham et al. is used in the current study to verify the model while maintaining the same dimensions, flow inlet, and boundary conditions. With an average inaccuracy of 4.47%, the current work is verified against the earlier work by Pham et al. [3]. If the error percentage was higher, the results would have been more inaccurate. So, while considering the results, it has to be remembered that the results are 4.47% erroneous than the actual ones. This emphasizes the reliability of the model. The model can

generate more accurate results if the errors are less. A water velocity of 1.43 m/s, air velocity of 0 m/s, water volume fraction of 99.06%, and air volume fraction of 0.94% are the intake conditions for the validation task.

RESULTS AND DISCUSSION

Water Volume Fraction 50%

Figure 5 shows the flow pattern of 50% VOF of water both for the horizontal-vertical orientation, and vertical orientation, respectively. The stratified flow is observed by the water and air interaction both moving at velocities of 3 m/s which is similar according to Baker's flow map. Here, the water phase is deflected by the centrifugal force to the bend effect which is clearly seen in both orientations. However, the liquid deposition downstream of the vertical pipe is more than the horizontal one due to the effect of gravitational deceleration. This deposition of liquid can create obstacles to maintaining the flow from the outlet of the pipe. So, the velocity of the flowing fluids must be high

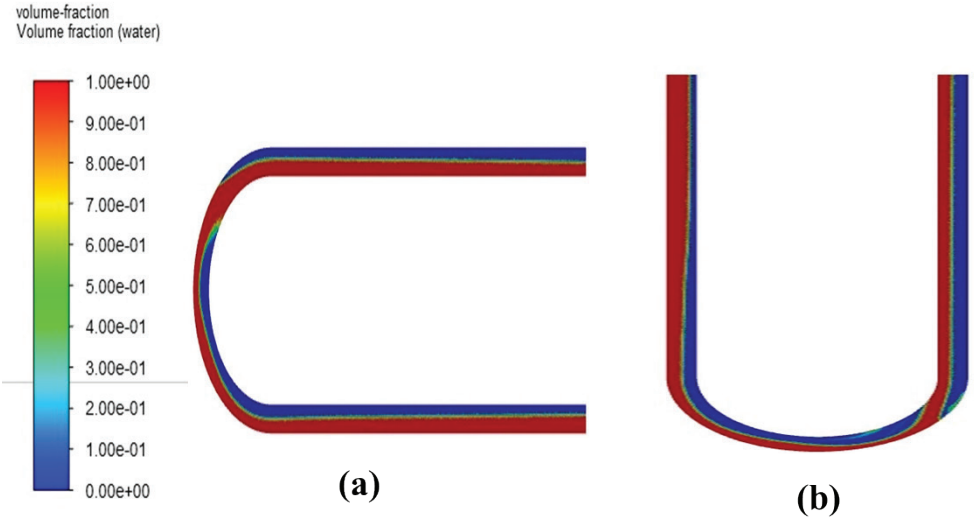

Figure 5. Flow pattern of 50% VOF of water: (a) horizontal-vertical orientation, and (b) vertical orientation.

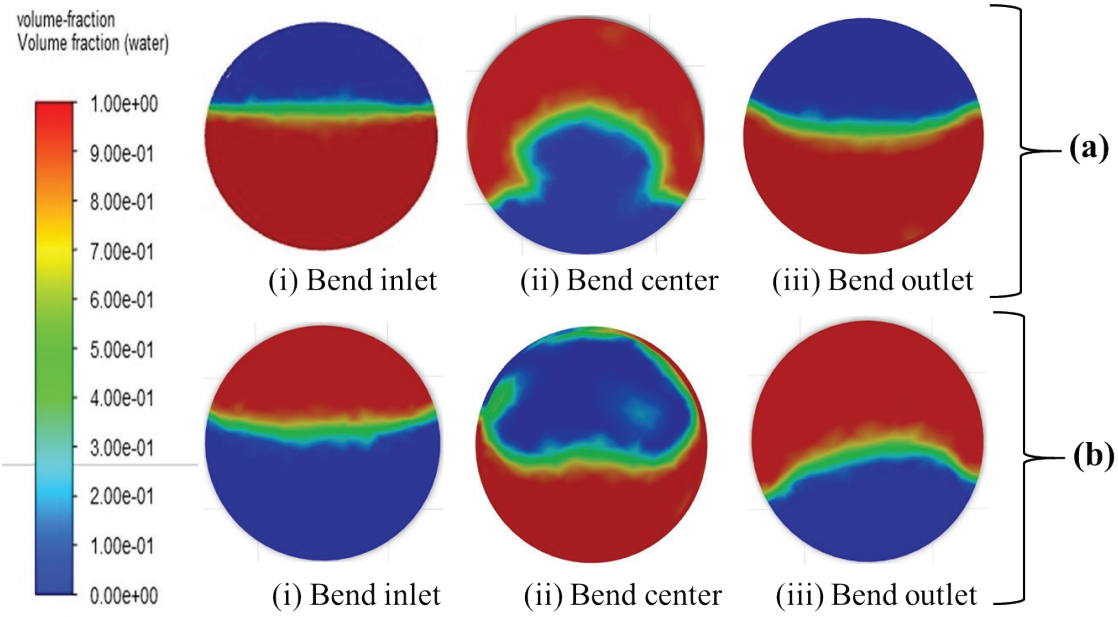

Figure 6. Phase distribution at the bend for 50% VOF of water: (a) horizontal-vertical orientation, and (b) vertical orientation.

enough to overcome this problem. Also, the flow behavior can show vorticity if the backflow pressure increases. Hence, the viscous effect is more at the downstream of the pipe than the upper stream.

Looking closely at Figure 6, it is evident at the bend's intake that there is a distinct interface between the phases of water and air, with more water distributed in the bottom half and air in the upper part for vertical-horizontal orientation and the opposite one is observed for the other orientation. The vertical pipe which has gravitational effect shows that the volume fraction of water is smaller to higher from bend inlet to bend outlet. However, the horizontal position shows quite a different view. The gravitational acceleration creates constricted passage at the inlet of the vertical position, unlike the horizontal position. Hence, these differences have occurred.

In Figure 7, the liquid holdup at the bend with a volume proportion of water of 50% has been depicted. After a fixed distance from the intake, the flow separation between the two phases occurs at both positions. The water phase has

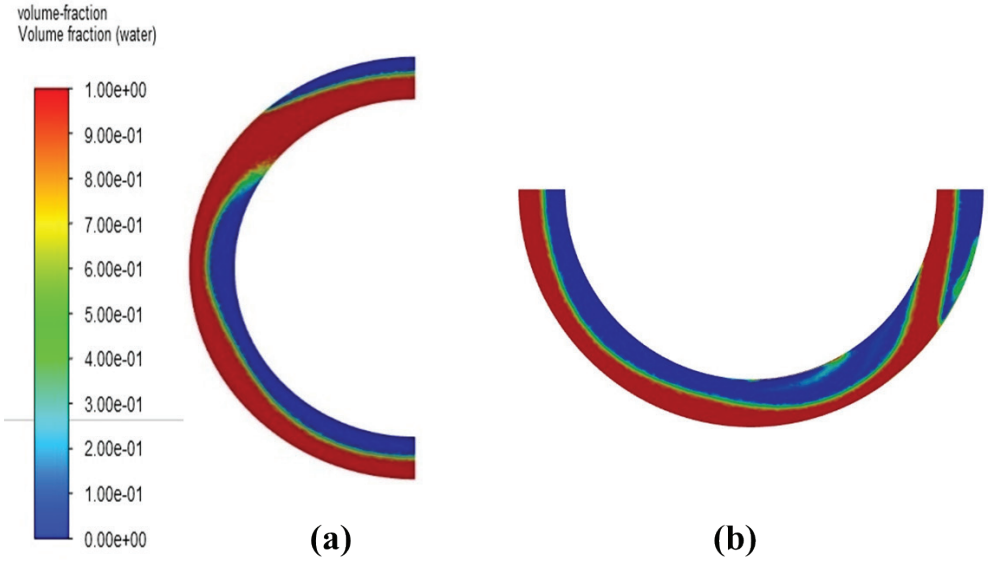

Figure 7. Liquid holdup for 50% VOF of water at the bend: (a) horizontal-vertical orientation, and (b) vertical orientation.

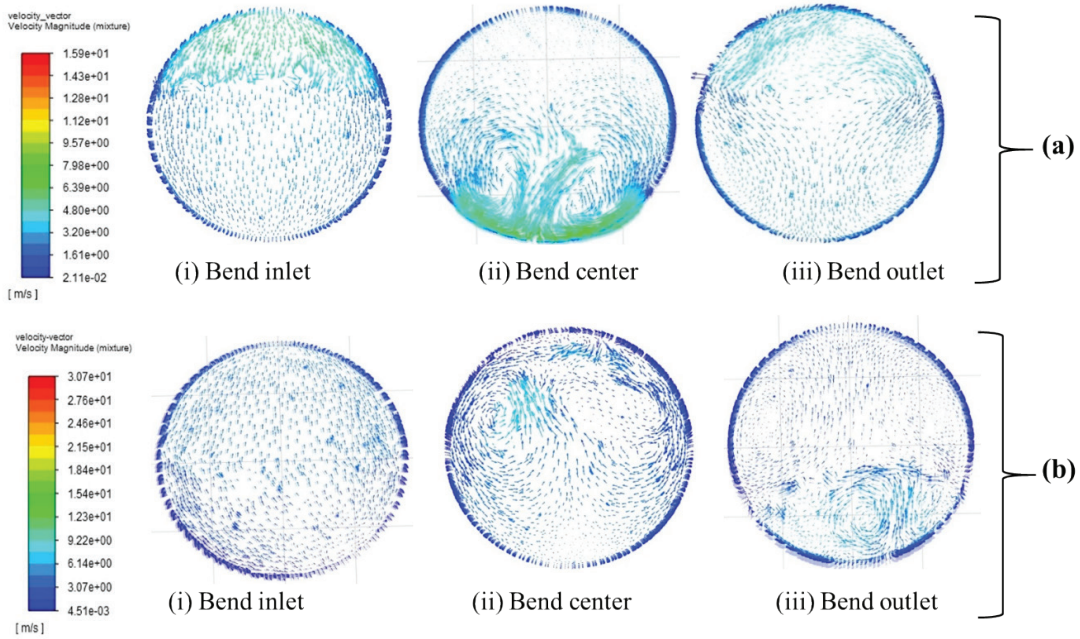

Figure 8. Velocity vector at the bend for 50% VOF of water: (a) horizontal-vertical orientation, and (b) vertical orientation.

splattered on the bends outside the wall, while the air phase flows towards the inner wall. Following flow separation, the liquid water is nearly equivalent to the air phase. Due to the separation of flow, the flow behavior shows vorticity and regions of wake. Hence, this causes more pressure losses throughout the pipe, unlike the straight pipe.

In Figure 8, the velocity vector is displayed at the bend. The flow at the bend inlet and center appears to be similar. The former shows smooth flow while the latter one vorticity called secondary flow. However, the velocity vector at the bend outlet of the vertical one shows discrepancies from the other one. This is perhaps due to the flow against gravity. The gravitational effect has less impact on the bend inlet and center for both orientations. However, the flow generates more vorticity in the horizontal position than the vertical one possessing a gravitational effect. Additionally, the velocity is higher at a bend of the vertical than the horizontal indicating more turbulence. The velocities are higher for the vertical pipe than the horizontal due to the gravitational effect in the former. The pressure distributions, shown in Figure 9, have given completely opposite results for both orientations. The static, dynamic, and total pressures in vertical orientation are more than the horizontal one. The static pressure seems to be lower in the horizontal orientation than in the vertical one. However, the dynamic pressure shows different outcomes. The constricted passage at the bend outlet of the horizontal position and at the bend

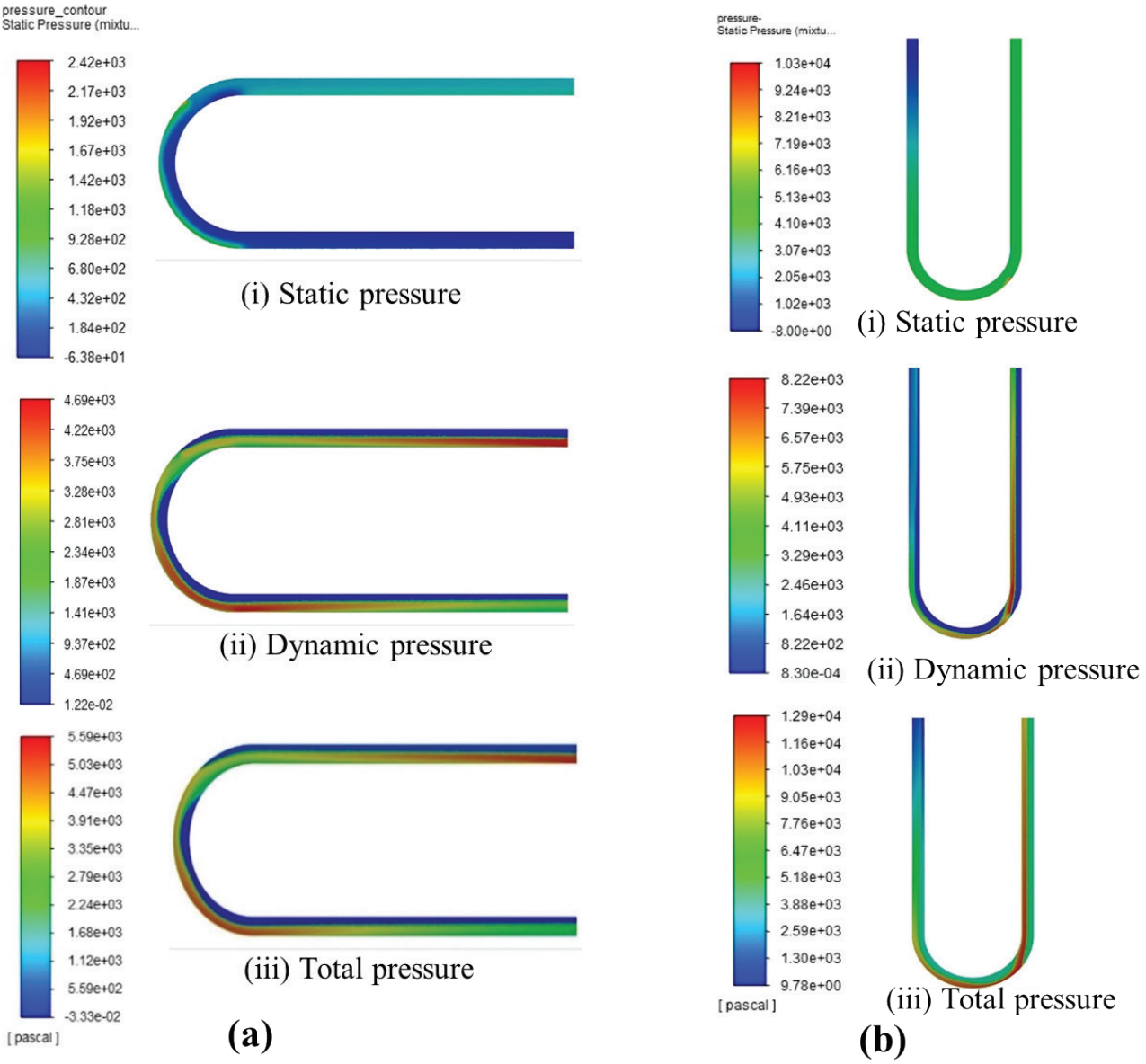

Figure 9. Variation of pressure along the U-bend tube for 50% VOF of water: (a) horizontal-vertical orientation, and (b) vertical orientation.

inlet of the vertical position generates more pressure. And, this has a significant effect on the total pressure as well.

Water Volume Fraction 70%

From Figures 10-14, the results have been shown for a 70% volume fraction of water. The results have given similar trends with the 50% volume fraction of water with the larger number. However, Figure 10 shows the flow pattern of 70% VOF of water both for the horizontal-vertical orientation, and vertical orientation, respectively, where the air-water interface gives a clear picture of wavy-stratified flow depicted in the figure. This is likely due to the similar flow pattern observed in Figure 5 with 50% VOF of water. However, the liquid occupies more portion of the pipe with 70% volume fraction than 50% volume fraction of water.

In Figure 11(a), the phase distribution at the bend inlet and outlet indicates similarity with Figure 6(a). And, air-water interface also matches the previous one. However, the bend center gives a different illustration. It is because it can be observed some tiny air-pockets for 70% VOF of water which is absent for 50% VOF. These air pockets can cause areas of lower pressure region and damage to the pipe. Again in Figure 11(b), the phase distribution of water is more as expected with the same phase distribution pattern with 50% VOF. But water droplets have been observed at the bend inlet unlike the Figure 5(b).

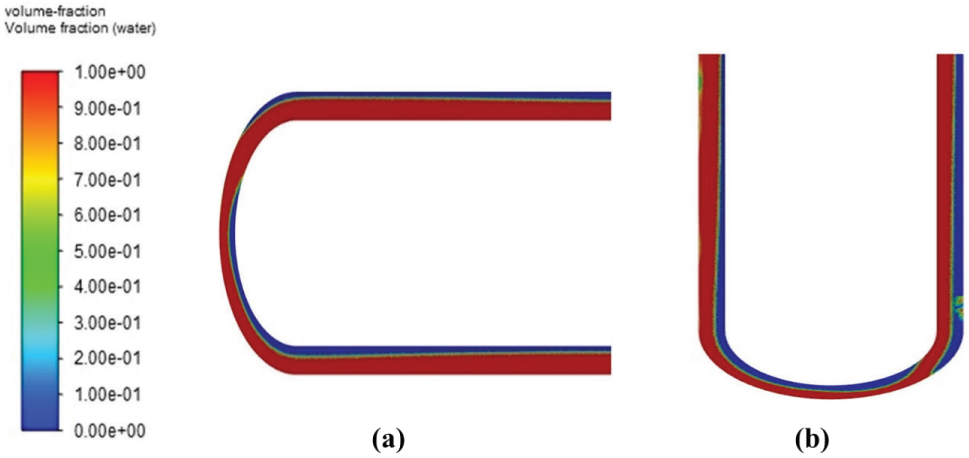

Figure 10. Flow pattern for 70% VOF of water (a) Horizontal-vertical, and (b)Vertical orientational.

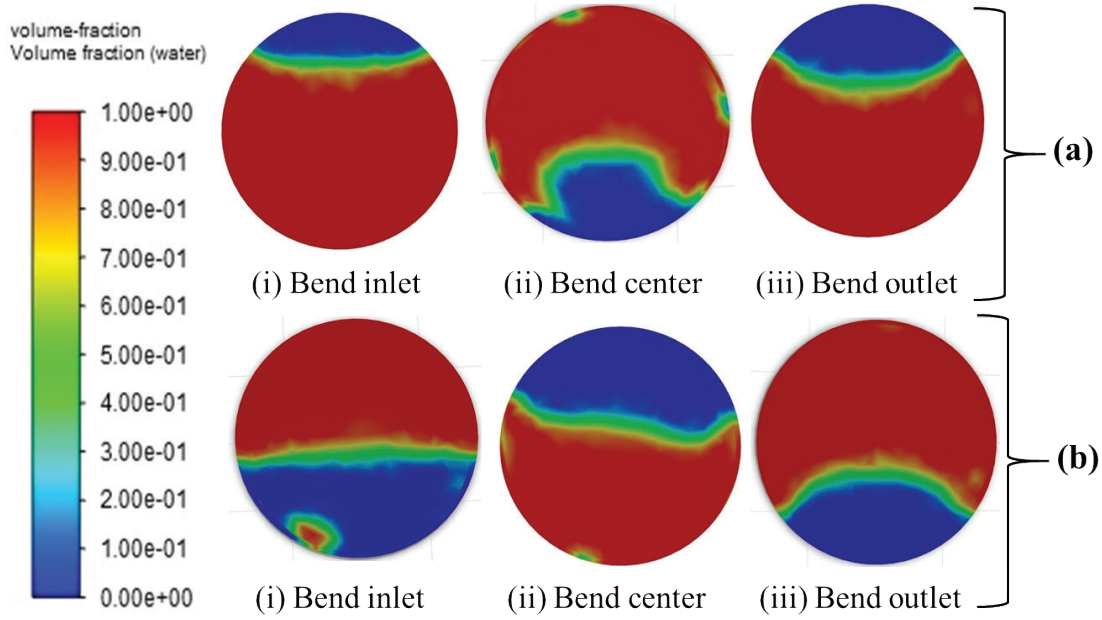

Figure 11. Phase distribution at the bend for 70% VOF of water: (a) Horizontal orientation, and (b) Vertical orientation.

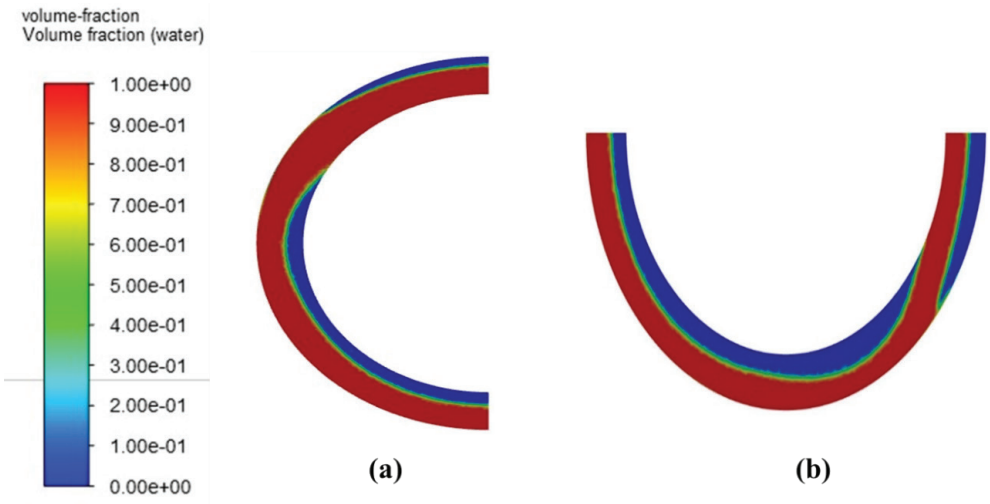

Figure 12. Liquid holdup for 70% VOF of water at the bend: (a) Horizontal-vertical orientation, and (b) Vertical orientation.

The liquid hold-up is almost the same for both the orientations of pipe. However, the effect of gravity is observed in Figure 12(b). The liquid hold-up is more for 70% VOF of water than 50 % VOF water in Figure 7. While the velocity vectors in Figure 13 for 70% VOF of water at the two orientations of the pipe have given the same results. Hence, the effect of increasing the water VOF is absolutely absent. However, though the mixture velocity increases, the turbulence has less effect on the velocity distribution. with 70% VOF of water. Comparing the static, dynamic, and total pressure in Figure 9 and Figure 14, very little (i.e., said to be no) significant changes have been detected other than the increased value of the pressure for 70% VOF water. Though the values have been increased for the static, dynamic, and total pressure, the impact on the flow behavior is less significant which can be observed from the other figures.

Pressure Variation

Figure 15 shows the pressure variation with U-bend pipe at different orientations: static pressure, dynamic pressure, and total pressure. The comparison of static pressure along the axial position of the pipe is shown in Figure 15(a). It can be clearly observed that the pressure is dropping at a higher value at the downstream part for the vertical orientation of the pipe than the horizontal-vertical one. This is due to the fact that the water which is the heavier fluid faces more viscous resistance for acceleration against gravity. As a result, the pressure drops at a larger number for the 50% and 70% VOF of water. However, at the bend inlet and center, the pressure is lowering steadily for both the position and VOF of water.

Dynamic pressure comparison has been depicted in Figure 15(b). The results are completely different in this case. For horizontal-vertical downflow for 50% and 70% VOF of water, the pressure decreases from pipe inlet to bend inlet. But the pressure tends to increase from the bend inlet and maximizes at the bend outlet due to a constricted passage as shown earlier in Figure 9 and Figure 14. After, the pressure again starts to decrease at the downstream portion. The pressure increases for the vertical downflow as the constricted passage of water has been observed which increases the pressure, from the pipe inlet to the bend inlet as given in Figure 9 and Figure 14. Then, the pipe bend faces a sudden drop of pressure following a small portion of the downstream of the pipe for both 50% and 70% VOF of water. After, the dynamic pressure tends to increase as there is a huge drop of static pressure described earlier in Figure15(a).

The total pressure variation is shown in Figure 15(c). The pressure variation for 50% and 70% VOF of water at horizontal-vertical downflow gives a similar trend as in the vertical pipe. But the pressure is lowered from the pipe inlet to bend for the horizontal-vertical downflow for both the VOF of water. On the contrary, the total pressure is slightly increasing due to the constricted passage of water created by the gravitational effect. Next, the total pressure variation is steady at the pipe bend and a small pressure drop follows the downstream part. However, the total pressure lowers with a great value starting from the pipe bend which has increased at the pipe downstream.

Figure 16 shows the pressure variation at the bend section of the u-bend pipe both for 50% and 70% of water for both orientations: horizontal-vertical and vertical. The pressure measurement at various bend angles has been illustrated in this figure. The bend angle has a negligible effect on horizontal-vertical and vertical downflow for 50% VOF of water. The curved lines are almost straight. However, with the higher bend angle and for 70% VOF of water, the pressure gives significant changes for both of the pipe positions. It may be due to the fact that higher VOF of water increases the liquid hold-up and thus, this causes the pressure to drop more.

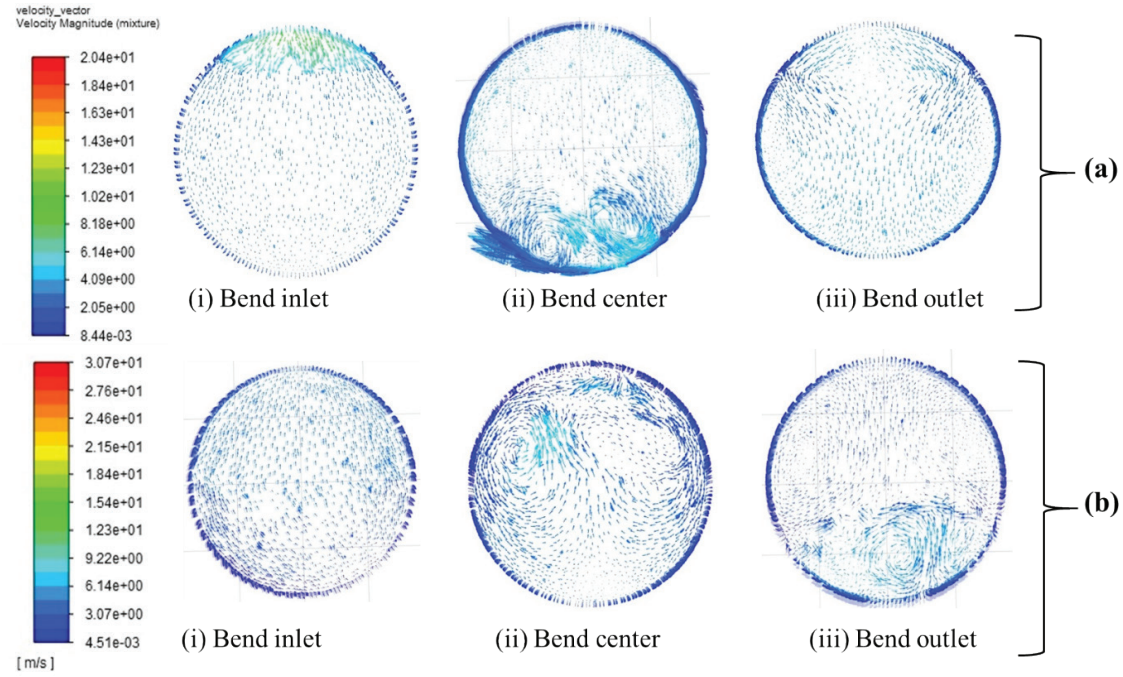

Figure 13. Velocity vector at the bend for 70% VOF of water: (a) Horizontal-vertical orientation, and (b) Vertical orientation.

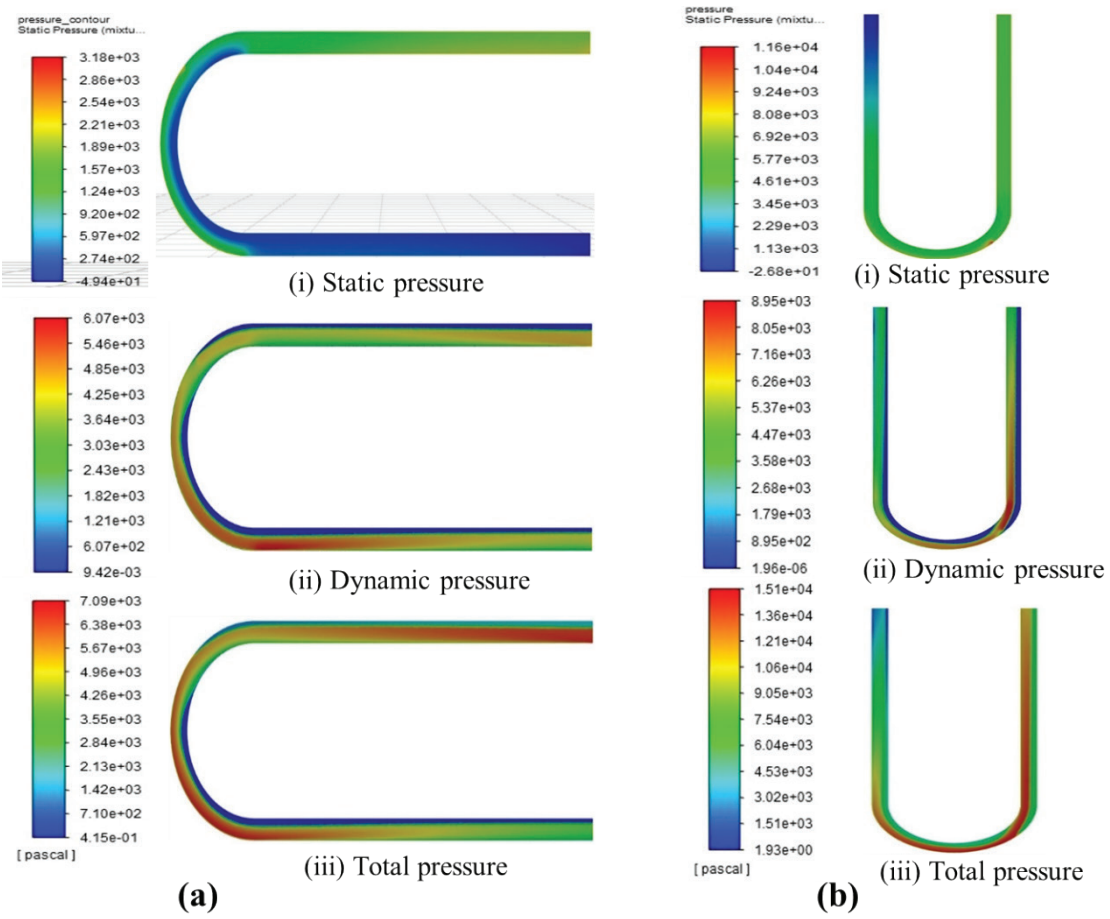

Figure 14. Variation of pressure along the U-bend tube: (a) Horizontal-vertical orientation, and (b) Vertical orientation.

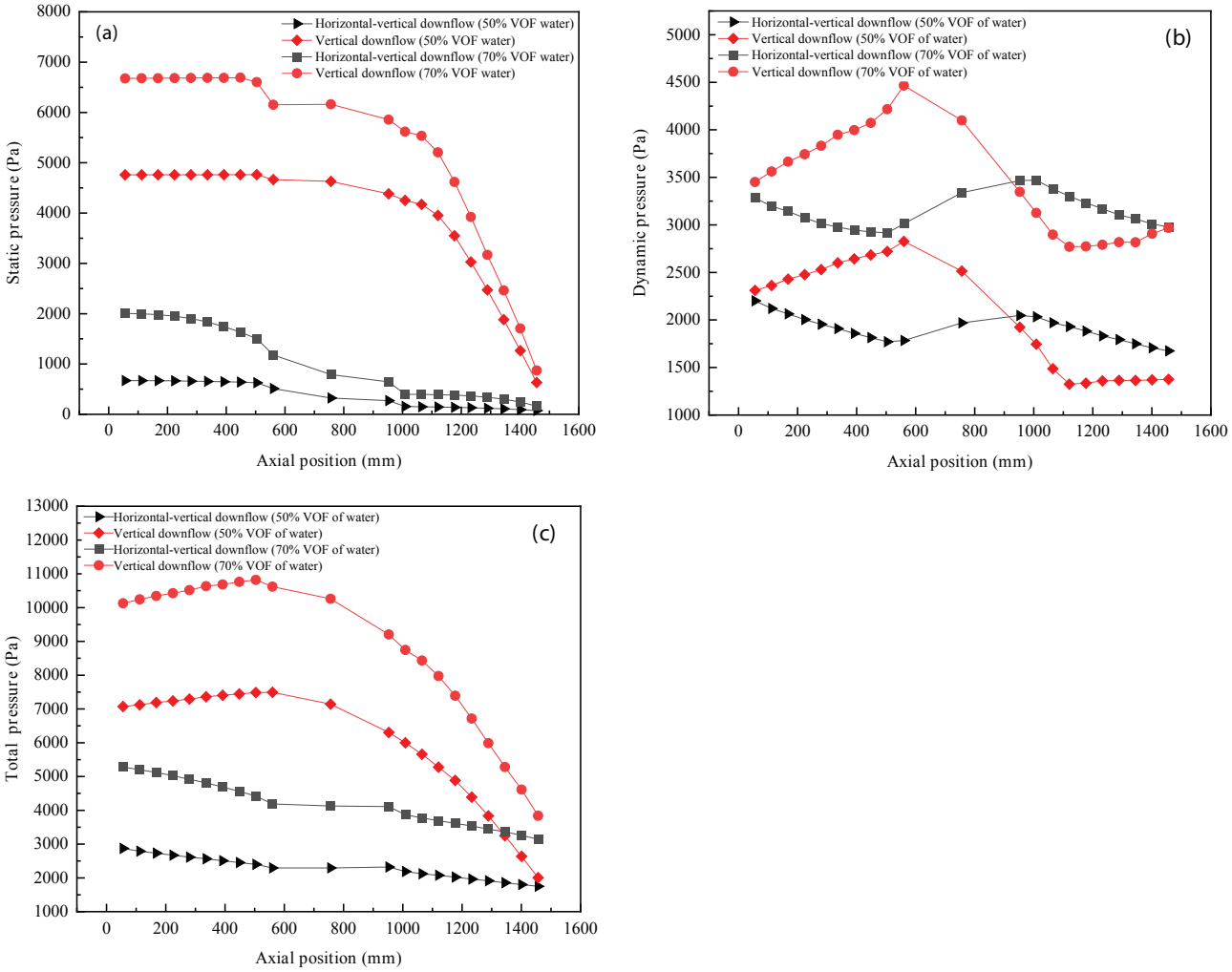

Figure 15. Pressure variation with U-bend pipe at different orientations: (a) static pressure, (b) dynamic pressure, and (c) total pressure.

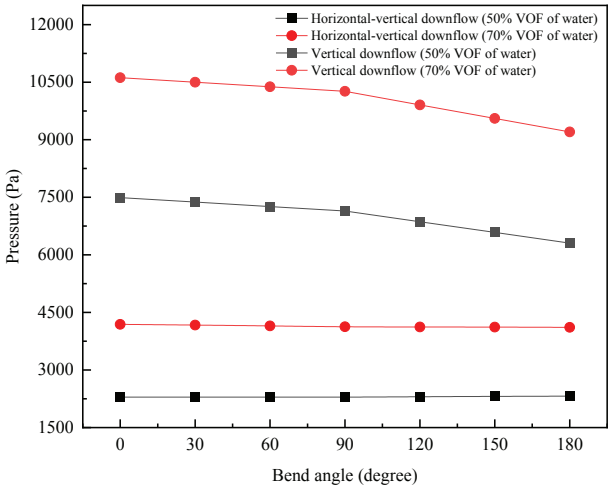

Figure 16. Pressure variation at the u-bend section both for 50% and 70% of water for both orientations: horizontal-vertical and vertical.

Figure 17 shows the comparison by considering the flow pattern of 50% VOF of water for the horizontal-vertical orientation. Figure 17(a) shows the comparison of water velocity at the bend inlet along with the axial length, where the mixture model for the two-fluid models is used to verify the model while maintaining the same dimensions, flow inlet, and boundary conditions by Pham et al. [3]. With an average inaccuracy of 4.47%, the current work is verified against the work of Pham et al. and hence, this emphasizes the reliability of the model. While, in Figure 17(b), the total pressure variation comparison has also been illustrated between Pham et al. [3] and the present work. The total pressure variation trends are similar for both of the works. However, the pressure curve for the present work varies slightly due to the differences in volume fraction with Pham et al. work. With a higher volume fraction, the total pressure magnitudes change, and the pressure loss is greater for the higher volume fraction which is depicted here. So, this comparison authenticates the results found through this study.

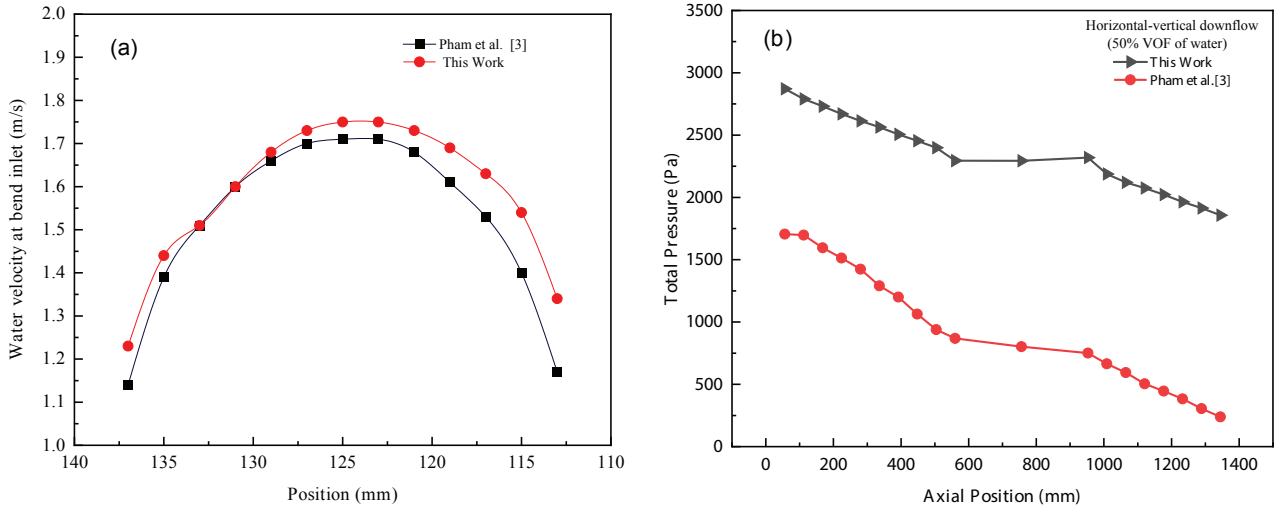

Figure 17. Illustration for comparing (a) water velocity at bend inlet, and (b) total pressure along the axial length.

CONCLUSION

The current investigation is conducted on the U-bend tube to see the flow pattern, examine how the bend affects the pressure drop for two types of pipe orientations, and determine the phase distribution. In summary, the subsequent findings have been discovered.

- The flow pattern for water and air inlet velocity of 3 m/s is observed in the stratified flow with very small wavy patterns at the interface of the air-water phase interactions for both orientations and volume fractions. This observation is consistent across both orientations and volume fractions, highlighting the impact of centrifugal and gravitational forces on phase interactions.
- The pressure drop is 1186 Pa and 1415 Pa for 50% and 70% volume fractions of water at the vertical downflow position of the pipe. On the other hand, an 80 Pa total pressure drop is found for a 70% volume fraction of water for the horizontal position of the U-shaped pipe. However, the pressure drop is negligible for a 50% volume fraction of water at the same orientation. This signifies that pressure losses increase with volume fraction.
- With higher volume fractions of water, the liquid hold-up at the bend increases due to the dominant centrifugal force over the gravitational force. This highlights the importance of considering phase distribution and flow patterns in U-bend pipes for efficient fluid transport in industrial applications.
- The pressure drops increase with the bend angle and the volume fraction of water.

The scope of this work can be extended to investigate whether air-water two-phase flow yields similar results with different types of refrigerants. Additionally, extensive studies in microchannels could provide valuable insights, allowing for comparison with current findings. In summary, this study shows that pipe orientation and water volume percentage have a considerable impact on the pressure drops and phase distributions in U-bend pipes. The results offer a fundamental insight that may guide fluid transport system design and optimization in a range of industrial settings.

NOMENCLATURE

α	Volume of fraction
A	Area
U	Superficial velocity
$\dot{Q}$	Flow rate
Δp	Total pressure drops
G	Mass flux
λ, ψ	Dimensionless parameters
ρ	Density
$\vec{v}$	Velocity
n	Surface normal correlated to the gradient of q^{th} volume fraction
θ	Angle
σ	Surface tension
S	User defined source term
U^*	Dimensionless velocity
y^*	Dimensionless distance from the wall
κ	Von Karman constant (0.4187)
E	Empirical constant (9.793)
U	Mean velocity
μ	Dynamic viscosity of the fluid
k	Turbulence kinetic energy
y	Distance from the centroid of the wall-adjacent cell to the wall

ACKNOWLEDGMENT

The authors appreciate and acknowledge the Khulna University of Engineering & Technology for providing high-performance computing facilities and other support throughout this work.

AUTHORSHIP CONTRIBUTIONS

Authors equally contributed to this work.

DATA AVAILABILITY STATEMENT

The authors confirm that the data that supports the findings of this study are available within the article. Raw data that support the finding of this study are available from the corresponding author, upon reasonable request.

CONFLICT OF INTEREST

The author declared no potential conflicts of interest with respect to the research, authorship, and/or publication of this article.

ETHICS

There are no ethical issues with the publication of this manuscript.

STATEMENT ON THE USE OF ARTIFICIAL INTELLIGENCE

Artificial intelligence was not used in the preparation of the article.

REFERENCES

[1] Hayashi K, Kazi J, Yoshida N, Tomiyama A. Pressure drops of air-water two-phase flows in horizontal U-bends. Int J Multiph Flow 2020;131:103403. [CrossRef]

[2] Dassler C, Janoske U. Numerical Investigation of Pressure Loss and Heat Transfer Characteristics in 180-Degree Bends. Heat Transf Eng 2023;44:803–822. [CrossRef]

[3] Pham TQ, Jeon J, Jo D, Choi S. Two-Phase Flow Simulations Using 1D Centerline-Based C- and U-Shaped Pipe Meshes. Appl Sci 2021;11. [CrossRef]

[4] Hayashi K, Yasui S, Kurimoto R, Tomiyama A. Void Fraction of Air-Water Two-Phase Flows in a Vertically Placed Horizontal U-Bend. Heat Transf Eng 2023;1–14. [CrossRef]

[5] Yadav S, Mehta HB. Experimental investigations on air–water two-phase flow through a minichannel U-bend. Exp Therm Fluid Sci 2016;78:182–198. [CrossRef]

[6] Usui K, Aoki S, Inoue A. Flow Behavior and Phase Distribution in Two-Phase Flow around Inverted U-Bend. J Nucl Sci Technol 1983;20:915–928. [CrossRef]

[7] Da Silva Lima RJ, Thome JR. Two-phase flow patterns in U-bends and their contiguous straight tubes for different orientations, tube and bend diameters. Int J Refrig 2012;35:1439–1454. [CrossRef]

[8] Deng D, Wang RS, Xie SW, Liu PP. Flow pattern and its transition of nitrogen gas–water two-phase flow in U-tubes and inverted U-tubes. Heat Mass Transf 2015;51:85–94. [CrossRef]

[9] Aliyu AM, Almabrok AA, Baba YD, Lao L, Yeung H, Kim KC. Upward gas–liquid two-phase flow after a U-bend in a large-diameter serpentine pipe. Int J Heat Mass Transf 2017;108:784–800. [CrossRef]

[10] Monachan B, Thomas RJ, Steaphen D, Skaria M, Shafi KA. Simulation of Stratified Two-phase Flow Regime using Air-Water Model in ANSYS Fluent®. J Phys Conf Ser 2019;1355:12014. [CrossRef]

[11] De Moerloose L, Vierendeels J, Degroote J. Effect of the liquid viscosity, wall wetting and mass flow rate on the flow through a horizontal U-bend subjected to an upwards flowing air-water mixture. 7th European Conference on Computational Fluid Dynamics. Glasgow;UK. 2018.

[12] Ma X, Liu T, Dai N, Tian M, Li S. Experimental Investigation on the Perturbation Length for Air–Water Flow Upstream and Downstream of U-Bends. Front Energy Res 2022;10:906809. [CrossRef]

[13] Mondol S, Hossain MI, Islam MT. Numerical Study of Water Flow through U-Bend Pipe. Available at: https://api.semanticscholar.org/CorpusID:211195619. Accessed on: 24 Mar 2026.

[14] Ghosh S, Das G, Das PK. Simulation of core annular in return bends—A comprehensive CFD study. Chem Eng Res Des 2011;89:2244–2253. [CrossRef]

[15] Bandyopadhyay TK, Das SK. Application of Computational Fluid Dynamics for Two-Phase Gas– Newtonian Liquid Flow through U-Bend. Int J Fluid Mech Res 2014;41. [CrossRef]

[16] Andrzejczyk R, Muszynski T. Experimental and comparative study on the two-phase pressure drop of air-water mixture in U-bend and straight pipe annuli. J Phys Conf Ser 2018;1101:12002. [CrossRef]

[17] Ogunsesan OA, Hossain M, Droubi MG. Computational fluid dynamics modelling of multiphase flows in double elbow geometries. Proc Inst Mech Eng Part E J Process Mech Eng 2021;235:1835–1846. [CrossRef]

[18] Ali SH, Eqqab MI. A computational study of curvature effect on pressure drop of gas-liquid two-phase flow through 90 degree elbow. Therm Sci 2022;26:3215. [CrossRef]

[19] Zahedi R, Rad AB. Numerical and experimental simulation of gas-liquid two-phase flow in 90-degree elbow. Alexandria Eng J 2022;61:2536–2550. [CrossRef]

[20] López J, Ratkovich N, Pereyra E. Analysis of two-phase air-water annular flow in U-bends. Heliyon 2020;6:e05818. [CrossRef]

[21] Lu C, Kong R, Qiao S, Larimer J, Kim S, Bajorek S, et al. Frictional pressure drop analysis for horizontal and vertical air-water two-phase flows in different pipe sizes. Nucl Eng Des 2018;332:147–161. [CrossRef]

[22] Abdulkadir M, Azzi A, Zhao D, Lowndes IS, Azzopardi BJ. Liquid film thickness behaviour within a large diameter vertical 180° return bend. Chem Eng Sci 2014;107: 137–148. [CrossRef]
[23] Nouri S, Hafsia Z, Boulaaras SM, Allahem A, Alkhalaf S, Feng B. Numerical Analysis of Stratified and Slug Flows. Math Probl Eng 2021;8418008. [CrossRef]
[24] Mahmood ASRA, Buttsworth D. CFD Numerical And Experimental Investigation Of Two-Phase Flow Development After An Expansion Device In A Horizontal Pipe. J Therm Eng 2021;7:307–323. [CrossRef]
[25] Karademir H, Ozcelik G, Acıkgoz O, Dalkılıc AS, Ince IT, Meyer J, et al. Comprehensive Review On The Flow Characteristics Of Two-Phase Flows In Inclined Tubes. J Therm Eng 2021;7:483–549. [CrossRef]
[26] Yaqop BN. Gas-liquid two-phase flow pressure drop in flattened tubes: an experimental and numerical study. J Therm Eng 2024;10:196–206. [CrossRef]
[27] Hamad FA, He S, Khan MK, Bruun HH. Development of kerosene–water two-phase up-flow in a vertical pipe downstream of A 90° bend. Can J Chem Eng 2013;91:354–367. [CrossRef]
[28] Spedding PL, Benard E, Mcnally GM. Two- and Three-Phase Flow Through a 90 Degree Bend. Dev Chem Eng Miner Process 2005;13:719–730. [CrossRef]
[29] Islam L, Mondal D, Islam MA, Das P. Effects of Heat Transfer Characteristics of R32 and R1234yf with Al2O3 Nanoparticle through U-Bend Tube Evaporator. J Eng 2024;9991809. [CrossRef]
[30] Jiang F, Wang Y, Ou J, Chen C. Numerical Simulation of Oil-Water Core Annular Flow in a U-Bend Based on the Eulerian Model. Chem Eng Technol 2014;37:659–666. [CrossRef]
[31] Ooms G, Pourquie MJBM, Westerweel J. Numerical study of laminar core-annular flow in a torus and in a 90° pipe bend. AIChE J 2015;61:2319–2328. [CrossRef]
[32] Ma K, Liu Z, Tang Y, Liu X, Yang Y, Yang S. Numerical investigation on ice slurry flow in horizontal elbow pipes. Therm Sci Eng Prog 2022;27:101083. [CrossRef]
[33] BS Onal, Akgul D, Mercan H, Dalkılıc AS, Wongwises S. Heat transfer and pressure drop characteristics of two phase flow in helical coils. Therm Sci Eng Prog 2022;27:101143. [CrossRef]
[34] Govier GW, Omer MM. The horizontal pipeline flow of air-water mixtures. Can J Chem Eng 1962;40:93–104. [CrossRef]
[35] Wang CC, Yang KS, Chang YJ, Lu DC. Characteristics of air–water two-phase flow in a 3-mm smooth tube. Can J Chem Eng 2000;78:1011–1016. [CrossRef]
[36] Wang CC, Chen IY, Yang YW. Influence of horizontal return bend on the two-phase flow pattern in a 6.9 mm diameter tube. Can J Chem Eng 2002;80:478–484. [CrossRef]
[37] Salim A, Fourar M, Pironon J, Sausse J. Oil–water two-phase flow in microchannels: Flow patterns and pressure drop measurements. Can J Chem Eng 2008;86:978–988. [CrossRef]
[38] Al-Hadhrami LM, Shaahid SM, Tunde LO, Al-Sarkhi A. Experimental Study on the Flow Regimes and Pressure Gradients of Air-Oil-Water Three-Phase Flow in Horizontal Pipes. Sci World J 2014;1:810527. [CrossRef]
[39] Patpatiya P, Samadder S, Kapoor V. Numerical Investigation of Two-Phase Flow in a Horizontal T Junction. Optimization of Industrial Systems. Beverly: Scrivener; Publishing; 2022. p. 85–99.
[40] Lightstone L, Osamusali SI, Chang JS. Gas-liquid two-phase flow in symmetrically dividing horizontal tubes. AIChE J 1991;37:111–122. [CrossRef]
[41] Nizovtseva IG, Starodumov IO, Schelyaev AY, Aksenov AA, Zhluktov SV, Sazonova ML, et al. Simulation of two-phase air–liquid flows in a closed bioreactor loop: Numerical modeling, experiments, and verification. Math Methods Appl Sci 2022;45:8216–8229. [CrossRef]
[42] Verma RK, Ghosh S. Two-Phase Flow in Miniature Geometries: Comparison of Gas-Liquid and Liquid-Liquid Flows. ChemBioEng Rev 2019;6:5–16. [CrossRef]
[43] Mondal D, Ikram MO, Rabbi MF, Moral MNA. Experimental Investigation and Comparison of Bend Tube Parallel & Counter Flow and Cross Flow Water to Air Heat Exchanger. Int J Sci Eng Res 2014;5:686–695.
[44] Mondal D, Alam A, Islam MA. Experimental Observation of a Small Capacity Vapor Absorption Cooling System. Int J Sci Eng Res 2014;5:456–467.
[45] Mondal D, Islam MA. Experimental Investigation on an Intermittent Ammonia Absorption Refrigeration. Mech Eng Res J 2018;11:59–65.
[46] Mondal D, Hori Y, Kariya K, Miyara A, Alam MJ. Measurement of Viscosity of a Binary Mixture of R1123 + R32 Refrigerant by Tandem Capillary Tube Method. Int J Thermophys 2020;41:1–20. [CrossRef]
[47] Mondal D, Kariya K, Tuhin AR, Amakusa N, Miyara A. Viscosity measurement for trans-1,1,1,4,4,4-hexafluoro-2-butene(R1336mzz(E)) in liquid and vapor phases. Int J Refrig 2021;133:267–275. [CrossRef]
[48] Mondal D, Kariya K, Tuhin AR, Miyoshi K, Miyara A. Thermal conductivity measurement and correlation at saturation condition of HFO refrigerant trans-1,1,1,4,4,4-hexafluoro-2-butene (R1336mzz(E)). Int J Refrig 2021;129:109–117. [CrossRef]
[49] Mondal D, Tuhin AR, Kariya K, Miyara A. Measurement of Kinematic Viscosity and Thermal Conductivity of 3,3,4,4,5,5-HFCPE in Liquid and Vapor Phases. Int J Refrig 2022;140:150–165. [CrossRef]

[50] Das P, Mondal D, Islam A, Afroj M. Thermodynamic performance evaluation of a solar powered Organic Rankine cycle (ORC) and dual cascading vapor compression cycle (DCVCC): Power generation and cooling effect. Energy Convers Manag X 2024;23:100662. [CrossRef]

[51] Arefin MM, Mondal D, Islam MA. Optimizing cascade refrigeration systems with low GWP refrigerants for Low-Temperature Applications: A thermodynamic analysis. Energy Convers Manag X 2024;24:100722. [CrossRef]

[52] Bari MA, Mondal D, Hasib MA. Impact of air flow, temperature distribution, and heat transmission in a refrigerator compartment with and without shelves: A numerical approach. J Therm Eng 2024;10:1590–1606. [CrossRef]

[53] Shaharier MT, Mondal D, Hasib MA, Islam MA. Effects of gas-liquid flow and dehumidification performance of a liquid desiccant dehumidifier: A numerical approach for vertical smooth & rough, and inclined rough plates. J Therm Eng 2024;10:1559–1576. [CrossRef]

[54] Sobamowo MG, Akinshilo AT. Analysis of flow, heat transfer and entropy generation in a pipe conveying fourth grade fluid with temperature dependent viscosities and internal heat generation. J Mol Liq 2017;241:188–198. [CrossRef]

[55] Akinshilo AT, Olaye O. On the analysis of the Erying Powell model based fluid flow in a pipe with temperature dependent viscosity and internal heat generation. J King Saud Univ Eng Sci 2019;31:271–279. [CrossRef]

[56] Akinshilo AT, Sobamowo GM. Perturbation Solutions for the Study of MHD Blood as a Third Grade Nanofluid Transporting Gold Nanoparticles through a Porous Channel. J Appl Comput Mech 2017;3:103–113.

[57] Seikh AH, Akinshilo AT, Taheri MH, Alharthi N, Khan I, Khan AR, et al. Influence of the nanoparticles and uniform magnetic field on the slip blood flows in arterial vessels. Phys Scr 2019;94:125218. [CrossRef]

[58] Ansys®, ANSYS Fluent Theory Guide, 2020th ed.

[59] Brackbill JU, Kothe DB, Zemach C. A continuum method for modeling surface tension. J Comput Phys 1992;100:335–354. [CrossRef]